SCIENTIFIC REPQRTS

OPEN

Frequency specific contribution of intrinsic connectivity networks to the integration in brain networks

Yeong-Hun Park [1], Jungho Cha[2], Viktoriya Bourakova[2] & Jong-Min Lee[1]

Brain networks are integrated and segregated into several intrinsic connectivity networks (ICNs). Frequency specificity of ICNs have been studied to show that different ICNs have a unqiue contribution to brain network integration along frequencies. The purpose of this study was to evaluate the contribution of individual ICN to brain network integration along their frequency. We used 14 ICNs and determined 2 frequency bands (LF1, 0.03~0.08 Hz and LF2, 0.009~0.012 Hz) from the hierarchical clustering of 101 frequency bins. We proposed a novel measure, called ICN efficiency, representing the difference between the global efficiencies of the whole brain network with and without the ICN to evaluate the contribution of the ICN to brain network integration. We found that each ICN had a different ICN efficiency at 2 frequency bands. We also found that the distinct subregions of the same ICN had a frequency specific contribution to brain network integration. Futhermore, the integration with other ICNs of the distinct subregions of the same ICN were different at 2 frequency bands. In conclusion, the contribution of each ICN to brain network integration is frequency specific and distinct subregions of the same ICN have functionally distinct roles with other ICNs at 2 frequency bands.

Functional connectivity (FC) is defined as the correlation of low frequency (0.009~0.08 Hz) fluctuations among anatomically distinct brain areas on resting-state functional magnetic resonance imaging (fMRI)[1]. FC has been widely used to gain insight into the fundamental functional architecture of the brain[2] and to identify intrinsic connectivity networks (ICNs), which are determined by spatially independent and temporally correlated FC[3]. There have been reported 10~14 ICNs associated with intrinsic functions such as vision, hearing, language, working memory, visuospatial attention, salience processing and episodic memory in the resting-state brain[4–10].

Several studies revealed specific frequencies for ICNs within the low frequency spectrum of blood oxygen level dependent (BOLD) signal and suggested that different ICNs likely have unique intrinsic frequencies[11–15]. Mantini, et al.[15] showed that 6 ICNs that fluctuate at slightly different BOLD signal frequencies were correlated with specific electrophysiological rhythms. Wu, et al.[14] showed that cortical networks concentrate within ultra-low frequency range (0.01~0.06 Hz), while connections within limbic networks distribute over a wider frequency range (0.01~0.14 Hz). Sasai, et al.[12] and Thompson and Fransson[13] showed the frequency specificity of ICNs from the viewpoint of whole brain network integration and segregation. Chen, et al.[11] demonstrated that ICN information of the slow-4 (0.027~0.073 Hz) and slow-5 (0.01~0.027 Hz) frequency bands are complementary in classifying between autism spectrum disorder and healthy controls. Among the low frequency divisions of previous studies (Table 1), the most used frequency bands are the slow-4 and slow-5 frequency bands of Zuo, et al.[16]. The criteria for slow-4 and slow-5 frequency bands were based on electro-physiological data from rats[17]. Observing the frequency specific contribution of ICN is an analysis in terms of the connectivity network, so it may be more appropriate to determine the frequency band based on connectivity matrix constructed using the BOLD signal rather than based on the electro-physiological frequency bands.

Brain networks combine to form one integrative complex network linking all brain regions and multiple ICNs together into one complex system[18]. Global and nodal efficiencies have been widely adopted to observe the integration of the brain network as graphical measures based on the shortest path length[19,20]. Sasai, et al.[12] evaluated the integration of a brain network composed of 3 ICNs using global efficiency and detected hubs by considering the nodal degree and eigenvector centrality. However, global and nodal efficiencies are insufficient to evaluate the contribution of each ICN to brain network integration because they are indicators for the overall network or

[1]Department of Biomedical Engineering, Hanyang University, Seoul, Korea. [2]Memory and Aging Center, Department of Neurology, University of California, San Francisco, San Francisco, CA, USA. Correspondence and requests for materials should be addressed to J.-M.L. (email: ljm@hanyang.ac.kr)

Previous studies	Frequency
Wu et al.[14]	Ultra-low frequency (0.01–0.06 Hz), Wider frequency (0.01–0.14 Hz)
Zuo et al.[16]	Slow-5 (0.01–0.027 Hz), Slow-4 (0.027–0.073 Hz)
Baria et al.[57]	LF (0.01–0.05 Hz), MF1 (0.05–0.10 Hz), MF2 (0.10–0.15 Hz), HF (0.15–0.20 Hz)
Sasai et al.[12]	Very low frequency band (0.01–0.03 Hz), Low frequency band (0.07–0.09 Hz)
Qian et al.[58]	IMF5 (0–0.015 Hz), IMF4 (0.01–0.025 Hz), IMF3 (0.025–0.05 Hz), IMF2 (0.05–0.11 Hz), IMF1 (0.11–0.22 Hz)
Thompson and Fransson[13]	F1 (0.016 Hz), F2 (0.028–0.037 Hz), F3 (0.071–0.08 Hz)

Table 1. The low frequency division in previous studies.

each node. Also, since the definition of functional integration is commonly based on the concept of a path[21], the hub defined by nodal degree and eigenvector centrality are insufficient to evaluate functional integration than the hub defined by path-based measures. Unlike Sasai, *et al.*, Thompson and Fransson[13] evaluated the contribution of an ICN to the integration of a brain network composed of 10 ICNs using the strength contribution and detected hubs by considering the betweenness centrality (BC) based on the concept of a path. However, this may also not be sufficient for evaluating the contribution of an ICN to the integration of the brain network because it is based on each edge's value over the sum of all edges and only considers the first degree of each node.

Separating an ICN from the whole brain network and computing its efficiency could not evaluate the contribution of the ICN in brain network integration properly. A general approach to measure the efficiency of a specific node is to calculate the inverse of the average shortest path length between the first neighbors of the node in the condition while excluding the node[19]. This approach is known as local efficiency and indicates how efficiently the node's first neighbor communicates when the node is removed. We applied the same concept to measure the efficiency of the ICNs and proposed a novel measure, called ICN efficiency (E_{ICN}), defined as the difference between the global efficiency and the efficiency of the whole brain network excluding the ICN. This could result in evaluating the contribution of an ICN to whole brain network integration.

The purpose of this study was to evaluate the contribution of an ICN to brain network integration using E_{ICN} along the frequency. First, the connectivity matrices along the frequency band were constructed from time-varying frequencies of the brain network consisting of 14 ICNs. Hierarchical clustering analysis was conducted to choose 2 frequency bands. E_{ICN} was calculated at each frequency band.

Results

Dividing the low frequency range into the frequency bands.
We divided the low frequency range into 101 bins to construct connectivity matrix at each bin. The average silhouette values for ward clustering were obtained as a function of k. The number of clusters were determined as 2 because the silhouette value was the highest when using k = 2 (Fig. 1b). (See Supplementary Fig. S1 and Table S1 for the silhouette value about the number of clustering iteration). The resulting frequency bands were LF1 (0.03~0.08 Hz) and LF2 (0.009~0.012 Hz) (Fig. 1c).

Changes of E_{ICN} along the frequency bands.
E_{ICN} was calculated to determine whether the contribution of ICNs to brain network integration differs along the frequency bands (Fig. 2 shows significant differences in t-values with Bonferroni correction (p < 0.005)). The number of BC hubs were plotted as the indicator of E_{ICN} together. Note that the statistically significant difference in E_{ICN} and the difference in the number of BC hubs were consistent in the Auditory network (AN), Default mode network (DMN), Salience network (SN) and Precuneus network (PCN). Most ICNs had a positive E_{ICN} value except that basal ganglia network (BGN) had a negative E_{ICN} value. There are 3 distinct groups according to the pattern of E_{ICN} values along the frequency bands; (1) higher at LF2 than at LF1: DMN, Language network (LN), Sensorimotor network (SMN), SN and Visuospatial network (VSN), (2) lower at LF2 than at LF1: BGN, Visual network (VN) and PCN, (3) similar at LF1 and LF2: AN and executive control network (ECN). These results suggest that the contribution of each ICN to brain network integration is frequency specific.

Different integration between distinct subregions of the same ICN along the frequency band.
Three well-known ICNs that can be divided into distinct subregions were determined and E_{ICN} was calculated along the frequency bands with 6 sub-ICNs: dorsal DMN (dDMN), ventral DMN (vDMN), left ECN (lECN), right ECN (rECN), posterior SN (pSN) and anterior SN (aSN) (Fig. 3 shows significant differences in t-values with Bonferroni correction (p < 0.008)). Note that the statistically significant difference in E_{ICN} and the difference in the number of BC hubs were consistent in dDMN, pSN and aSN. The dDMN showed greater E_{ICN} at LF2, but the vDMN showed a similar E_{ICN}. The rECN showed greater E_{ICN} at LF2, but the lECN showed a similar E_{ICN}. The pSN and aSN showed greater E_{ICN} at LF2. These findings show that the distinct subregions of the same ICN had a frequency specific contribution to integration of brain network.

In addition, the efficiency between each sub-ICN and the other ICNs ($E_{ICN-ICN}$) was calculated along the frequency bands (Fig. 4). Comparing each sub-ICN pair, the vDMN showed a greater $E_{ICN-ICN}$ with other ICNs except for DMN and LN than dDMN at LF1. However, the vDMN showed a greater $E_{ICN-ICN}$ with AN, VN, SN, PCN and VSN than dDMN at LF2. The lECN showed a greater $E_{ICN-ICN}$ with DMN, VN, LN, SN,PCN and VSN than rECN at LF1. However, the lECN showed not difference in $E_{ICN-ICN}$ with all other ICNs compared from rECN at LF2. The aSN showed a greater $E_{ICN-ICN}$ with AN, BGN, DMN, LN, ECN, SN and PCN than pSN at LF1.
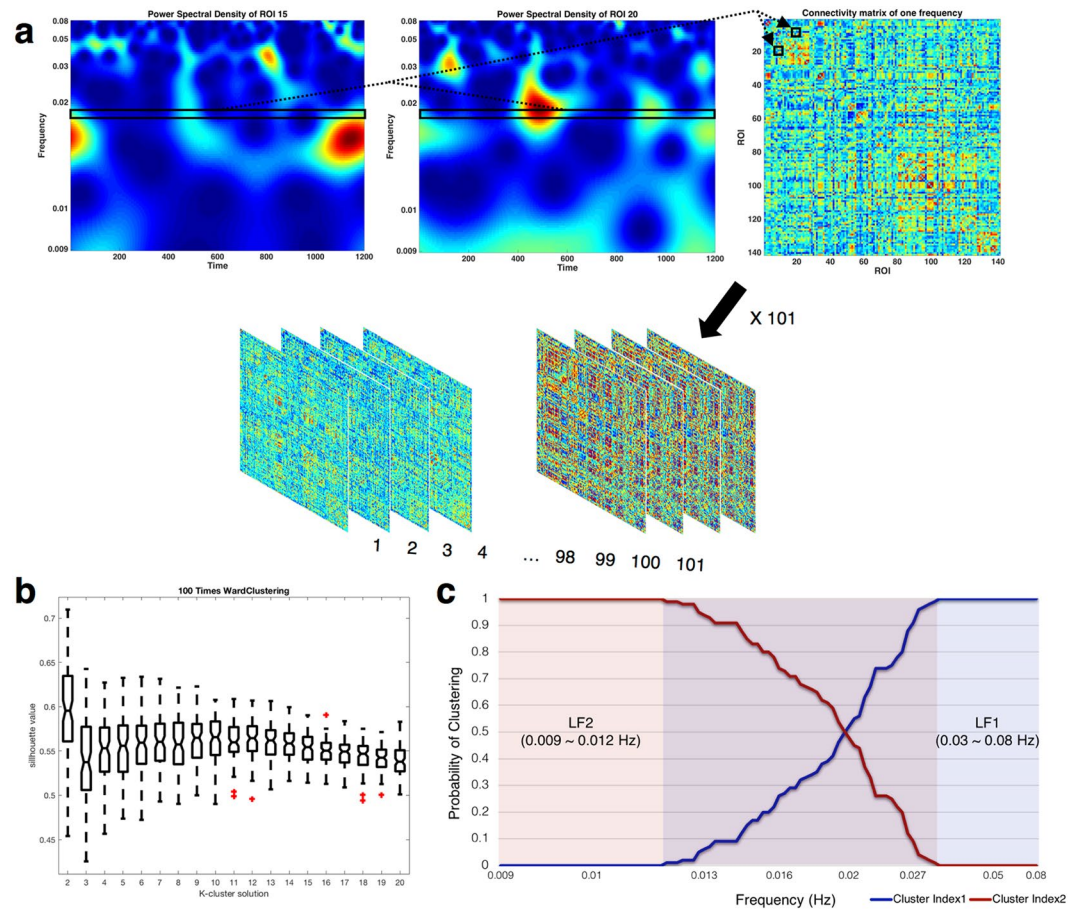
Figure 1. Construction of the connectivity matrix and division frequency bands. (**a**) A connectivity matrix was constructed for each frequency bin by using Pearson's correlation coefficient of each power spectral density (PSD) time-course through all nodes. The black rectangular small box indicates PSD time-course of specific frequencies. A 141 × 141 connectivity matrix of specific frequencies with a total of 101 frequency bins is presented. (**b**) The hierarchical clustering between group averaged connectivity matrices of each frequency was calculated by using Jensen Shannon divergence. For the highest silhouette value, 101 frequency matrices were clustered into 2 subbands. (**c**) Probability of clustering index for each frequency bin. Since the probability of the intermediate frequency band is uncertain, only the frequency bands at both ends were defined as the final 2 subbands (LF1: 0.03–0.08 Hz, LF2: 0.009–0.012 Hz).

However, the aSN showed a greater $E_{ICN-ICN}$ with SN than pSN at LF2. The difference in results was corrected with Bonferroni correction ($p < 0.0025$). The results suggested that the efficiency of each sub-ICN pair with the other ICNs is more different at LF1 than at LF2.

Consistent tendency of E_{ICN} to frequency of other data sets.

The E_{ICN} was calculated in two data sets to prove that the results of E_{ICN} are not data set dependent. When the E_{ICN} results of Human Connectome Project (HCP) S900 data and Beijing Normal University (BNU) data were compared, the results of BNU data differed from the results of HCP data in statistical significance of DMN, VN, SMN, PCN and VSN, but the tendency of E_{ICN} to frequency was maintained (Fig. 5a). Although there was a statistical difference, the tendency of E_{ICN} to frequency of BNU data was the same as the tendency of E_{ICN} to frequency of HCP data. This result indicates that ICN's frequency-specific contribution to the integration in brain networks is robust. In addition, when the 6 sub-ICN efficiency results of HCP data and BNU data were compared, the statistical tendency of sub-ICN did not reverse (Fig. 5b).

Discussion

In this study, we showed that ICNs make frequency specific contributions to the integration within the brain network (Fig. 2) and that the distinct subregions of the same ICN showed different characteristics along the frequency bands (Figs 3 and 4).

We determined 2 frequency bands (LF1, 0.03~0.08 Hz and LF2, 0.009~0.012 Hz) by hierarchical clustering which considered the FC matrix based on the BOLD signal. The FC frequency bands were slightly different from the electro-physiological frequency bands (slow-4, 0.027~0.073 Hz and slow-5, 0.01~0.027 Hz). The slow-4 range was included in LF1 and the slow-5 range was overlapped with LF2. Zuo, *et al.*[16] showed that slow-4 fluctuations
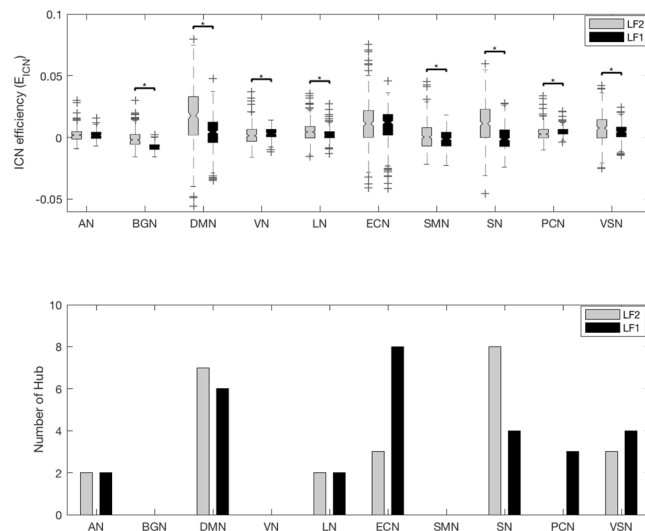
Figure 2. E_{ICN} and number of BC hubs along the frequency band. The E_{ICN} of the 10 ICNs was compared using a paired sample t-test analysis between the 2 frequency bands. The results were corrected by Bonferroni correction ($p < 0.005$). The tendency of E_{ICN} and number of BC hubs along the frequency bands were different for each ICN. The tendencies of E_{ICN} and number of BC hub along the frequency bands were similar in AN, DMN, SN and PCN. The abbreviations used were as follows: auditory network (AN), basal ganglia network (BGN), default mode network (DMN), visual network (VN), language network (LN), executive control network (ECN), sensorimotor network (SMN), salience network (SN), precuneus network (PCN), visuospatial network (VSN).
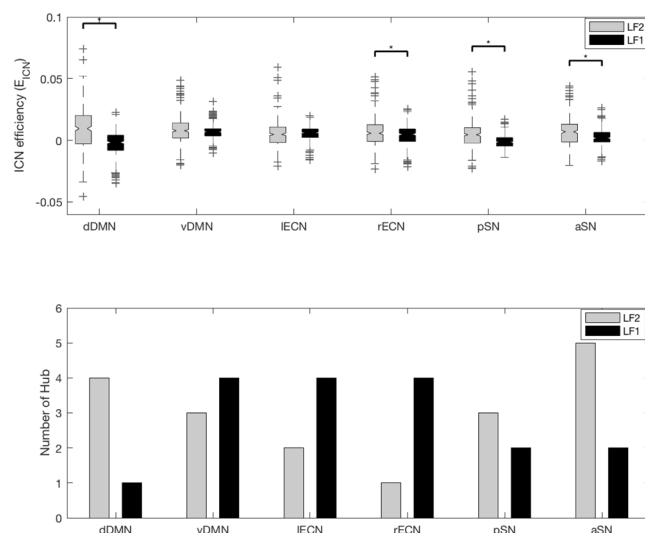
Figure 3. E_{ICN} and number of BC hubs along the frequency band. The E_{ICN} of the 6 sub-ICNs was compared using a paired sample t-test analysis between the 2 frequency bands. The results were corrected by Bonferroni correction ($p < 0.008$). The tendency of E_{ICN} and number of BC hubs along the frequency bands were different for each ICN. The tendencies of E_{ICN} and number of BC hub along the frequency bands were similar in dDMN, pSN and aSN. The abbreviations used were as follows: dorsal default mode network (dDMN), ventral default mode network (vDMN), left executive control network (lECN), right executive control network (rECN), posterior salience network (pSN) and anterior salience network (aSN).

are higher in the subcortical regions and several sensorimotor regions than slow-5 and slow-4 fluctuations are lower in the ventromedial regions than slow-5. Since then, many clinical studies of neurological and psychiatric disease[11,22–24] have used slow-4 and slow-5 to reveal regions of different brain activity from normal controls. Although many significant results were observed using slow-4 and slow-5, the slow-frequency bands are pre-defined frequency bands based on electro-physiological data from rats[17], as mentioned earlier. Therefore, it was necessary to find the frequency band by considering the FC matrix, and the LF1 and LF2 we obtained could be considered as fine-tuned frequency bands from slow-4 and slow-5 frequency bands. In future studies, it is better to use the fine-tuned frequency bands LF1 and LF2 than to use the slow-4 and slow-5 frequency bands when
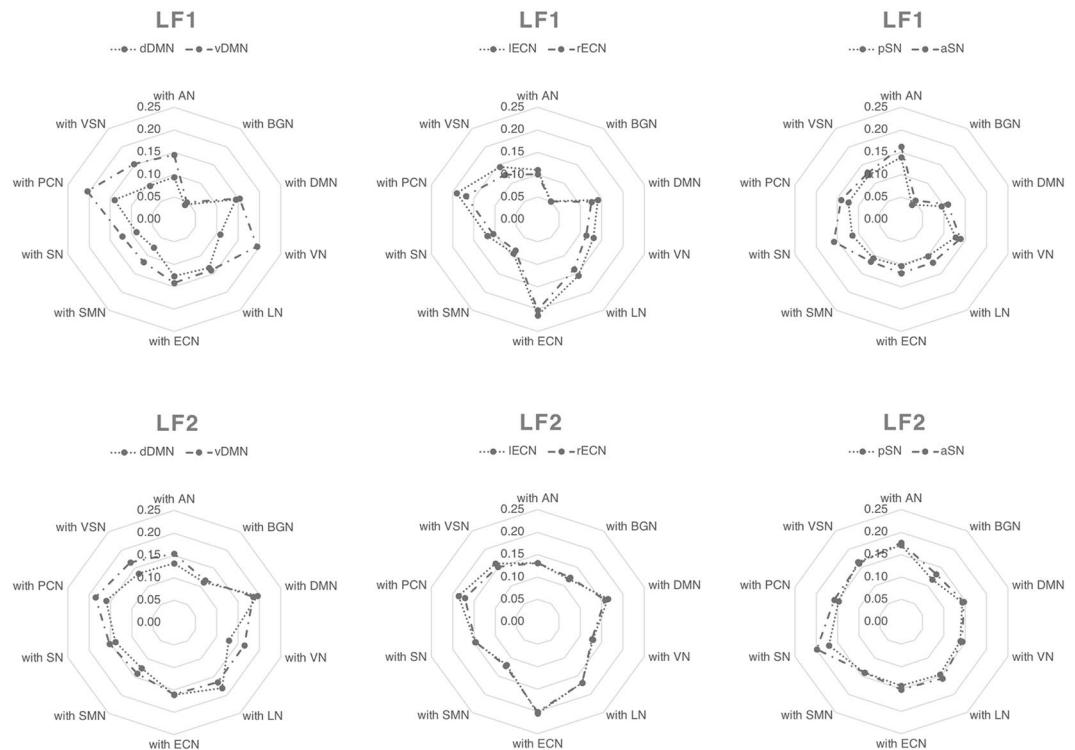
Figure 4. $E_{ICN-ICN}$ between sub-ICN and other ICN along the frequency band. The $E_{ICN-ICN}$ were calculated at LF1 and LF2. The patterns of $E_{ICN-ICN}$ were mainly different at LF1. The results were corrected by Bonferroni correction (p < 0.0025). The abbreviations used were as follows: dorsal default mode network (dDMN), ventral default mode network (vDMN), left executive control network (lECN), right executive control network (rECN), posterior salience network (pSN), anterior salience network (aSN) auditory network (AN), basal ganglia network (BGN), visual network (VN), language network (LN), sensorimotor network (SMN), precuneus network (PCN), visuospatial network (VSN).

analyzing frequency-specific brain networks rather than analyzing frequency-specific brain activity measured by amplitude of low frequency fluctuation.

We proposed E_{ICN} as a novel network measure for evaluating the contribution to brain network integration. While the global efficiency represents the integration of the whole brain and strength contribution considers the first degree neighbors only[12,13], E_{ICN} is a path-based method which considers whole brain network nodes as a quantitative indicator of the contribution of ICN to the integration of the whole brain network. The fact that E_{ICN} changes along frequency bands illustrates how the contribution of an ICN to brain network integration differs across frequency (Fig. 2). Note that each ICN had a different pattern of E_{ICN} values along frequency, which is similar to the frequency characteristics of each ICN observed through strength contribution in another study[13]. E_{ICN} of BGN had a negative result at all frequencies. Although BGN is known to have FC with other regions of the cortex[25], the results indicate that BGN interferes with brain network integration, therefore, more research about the contribution of BGN to brain network integration is needed.

We examined E_{ICN} with sub-ICN of three ICN along frequency bands to investigate different integrations between distinct subregions of the same ICN along the frequency band (Fig. 3). We also calculated $E_{ICN-ICN}$ with sub-ICN of three ICN to investigate different integrations with other ICNs (Fig. 4). A central component of the DMN resides in the posterior cingulate cortex (PCC), which is functionally correlated and separated into dorsal and ventral areas by cytology[26]. The dorsal PCC is strongly functionally connected with the DMN and with the cognitive control network (CCN), which is typically involved in the control of externally directed behavior, while the ventral PCC is more strongly integrated with the DMN[27–29]. In our study, the dDMN and vDMN had a different E_{ICN} along the frequency band. The vDMN showed a larger $E_{ICN-ICN}$ with other ICNs than dDMN at LF1. This suggests that the vDMN integrates with other ICNs more than dDMN at LF1. To the best of our knowledge, this study is the first to demonstrate that distinct subregions of DMN play functionally distinct roles with the other ICNs in the frequency domain. The lECN and rECN showed a different E_{ICN} along the frequency band in spite of having the same region of interest (ROI) in the corresponding hemisphere. The lECN and rECN are known to associate different temperaments in motivation[30], which is probably related to the observation that the lECN showed a larger integration with other ICNs than rECN at LF1. The SN is divided into the aSN and pSN by structural and functional connectivity with the anterior and posterior insula[31,32]. The aSN and pSN had the same number of BC hubs at LF1, but the aSN showed a larger integration with other ICNs than pSN at LF1. The aSN plays a critical role in switching between the ECN and DMN[33], which may be one of the explanations for the aSN showing a larger $E_{ICN-ICN}$ with the DMN and ECN than pSN at LF1. From these observations we confirm that
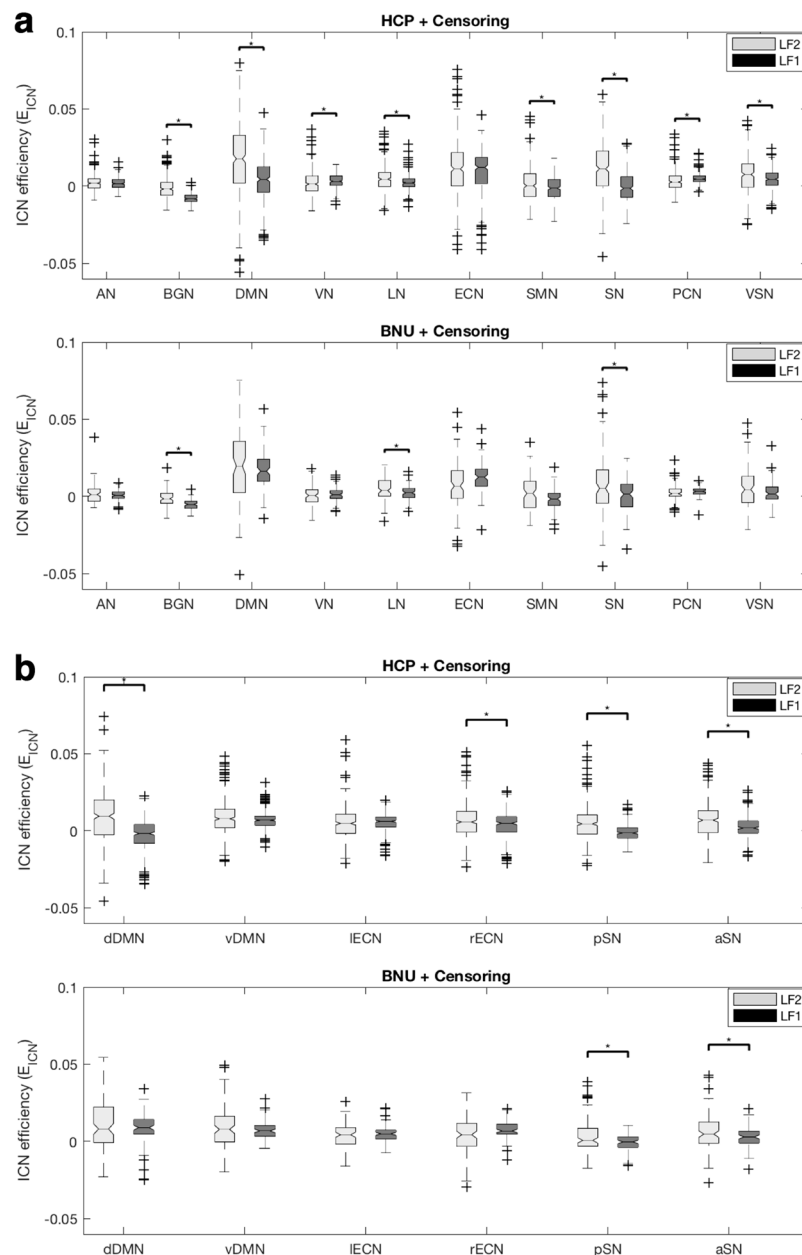
Figure 5. Impact of the data set on E_{ICN} by frequency. (**a**) Difference of E_{ICN} by frequency according to the data set. The E_{ICN} result of BNU data differ from the E_{ICN} results of HCP data in statistical significance of DMN, VN, SMN, PCN, and VSN, but the tendency of E_{ICN} to frequency is maintained. (**b**) Difference of E_{ICN} of 6 sub-ICN by frequency according to the data set. The statistical tendency of sub-ICN not reverse. The abbreviations used were as follows: dorsal default mode network (dDMN), ventral default mode network (vDMN), left executive control network (lECN), right executive control network (rECN), posterior salience network (pSN), anterior salience network (aSN), auditory network (AN), basal ganglia network (BGN), visual network (VN), language network (LN), sensorimotor network (SMN), precuneus network (PCN), visuospatial network (VSN).

the DMN and ECN are integrated centering on the aSN at LF1, indicating the frequency specificity of ICN to the integration in the brain network.

The present study has several limitations. First limitation is that different pre-processing methods lead to slightly different results (See Supplementary Fig. S2). The E_{ICN} results of three pre-processing pipelines differed from each other in statistical significance, but the tendency of E_{ICN} to frequency was maintained. These results indicate that the censoring step and global signal regression (GSR) step do not necessarily impact the magnitude of E_{ICN} along the frequency. In the end, we decided to include the preprocessing step by determining whether it was necessary or not, rather than judging whether the result was right or wrong. Therefore, we included the censoring step because it was necessary to exclude the large motion effect from the BOLD signal. However, the GSR step was not included because it was assumed that the nuisance-signal was already sufficiently removed

in the ICA-fixed step. Second limitation is selection of hyperparmeters for the Morlet wavelet transform. An angular frequency $\omega_0 = 6$, known to provide a good tradeoff between time and frequency localization, was set as in the previous[13,34–36]. For other hyperparameters, there was no information to set by reference. Nevertheless, our purpose was not to compare each frequency bin, but to compare the frequencies after clustering them into subbands, so we have compared clustering results under various conditions (See Supplementary Fig. S3). When the frequency clustering results are compared by changing the smallest scale 's_0' and spacing between scales 'ds', cluster colution 2 had the highest silhouette value under any conditions.

Methods

fMRI data.   The present study used HCP S900 data (http://humanconnectome.org/) released in December 2015[37]. In the HCP S900, 352 subjects (178 females and 173 males, age 22–36) were selected after excluding twin subjects for further analysis. The experiments were performed in accordance with relevant guidelines and regulations and all experimental protocol was approved by the Institutional Review Board (IRB) (IRB # 201204036; Title: 'Mapping the Human Connectome: Structure, Function, and Heritability'). Written informed consent was obtained from all participants. Our data analysis was performed in accordance with ethical guidelines of the Hanyang University ethics committee. Data were collected on a customized Siemens 3 T Connectome Skyra magnetic resonance imaging (MRI) with a standard 32-channel head coil at the Washington University in St. Louis. Echo planar imaging (EPI) time-series scans consisted of 1200 volumes and lasted for approximately 15 minutes with the following imaging parameters: TR = 720 ms; TE = 33.1 ms; flip angle = 52°; field of view = 208 × 180 mm^2; matrix size = 104 × 90; a multiband factor of 8; 72 slices; with voxel dimension = 2 × 2 × 2 mm^3. Participants were instructed to rest with their eyes open with relaxed fixation on a projected bright cross hair on a dark background during each scan. We used 'ICA-FIX cleaned' resting-state fMRI data only, which was preprocessed for co-registration, normalization, head motion correction, and artifact rejection[38,39]. The ICA-FIX cleanup preprocessing step regressed out non-neural contributions from fMRI data. The non-neural contributions are motion-related timecourses and artefact components identified using independent component analysis (ICA) with a new FSL tool FIX (FMRIB's ICA-based X-noisfier)[40]. For the additional pre-processing step, volume censoring was applied by using the frame-to-frame displacement (FD) method[41]. If the FDs exceeded a threshold of 0.35 at a time point, the time points values were censored and replaced by interpolated neighboring non-censored values. 51% of the total data included the censoring volume, with an average 13.2 out of 1200 volumes (1.1% of the fMRI data per subject). Among them, the censored volume ratio of two data were 25% and 35.91% respectively, and the analysis was carried out with a total of 350 data excluding the two data. We didn't include the GSR step because the 'ICA-FIX cleaned' data was already sufficiently regressed out the nuisance signals and the GSR step had a controversy[42]. We repeated the E$_{ICN}$ using the State Key Laboratory of Cognitive Neuroscience and Learning at BNU (n = 100), which is part of the 1,000 Functional Connectomes Project (http://fcon_1000. projects.nitrc.org/)[43]. The BNU EPI time-series scans consisted of 225 volumes and lasted for 7.5 minutes with the following imaging parameters: TR = 2000 ms; 33 slices; with voxel dimension = 3.125 × 3.125 × 3.6 mm^3. The fMRI data pre-processing proceeded according to our previous study[28,44–48]. The pre-processing included despiking, slice-timing, head motion correction, ANATICOR method[49] and volume censoring.

Constructing the nodes of the brain network.   We selected 141 functional ROIs as nodes covering 14 ICNs consisting of the AN, BGN, dDMN, vDMN, higher VN (hVN), primary VN (pVN), LN, lECN, rECN, SMN, aSN, pSN, PCN and VSN[9] from 499 functional ROIs originally defined by Richiardi, et al.[50].

Constructing the connectivity matrix.   We decomposed the averaged preprocessed time-series within each ROI into the time-frequency domain by convolving them with the complex Morlet wavelet function[51] and obtained power spectral density (PSD) maps by calculating the square of the magnitude of the continuous wavelet transform coefficient across time. For the Morlet wavelet, the hyperparmeters were used as follows: angular frequency $\omega_0 = 6$, smallest scale $s_0 = 1$, spacing between scales $ds = 1$, and number of scales $NbSc = 128$. We generated 101 frequency bins with a frequency resolution of roughly 0.001 Hz in the low frequency range (0.009~0.08 Hz) and constructed a connectivity matrix for each frequency bin using the Pearson's correlation coefficient among the PSD time-courses of the nodes (Fig. 1a).

Dividing the low frequency range into frequency bands.   We randomly selected 100 subjects from the 350 HCP subjects and constructed a group connectivity matrix with 101 frequency bins. The differences among the group-averaged connectivity matrices of each frequency bin were calculated using Jensen Shannon divergence[52,53]. The hierarchical clustering of connectivity matrices along the frequency band was performed to cluster the 101 frequency bins. We repeated the above procedure 100 times. The average silhouette values for ward clustering were obtained as a function of k (Fig. 1b). Since the silhouette value was highest when using k = 2, the frequency bins were clustered into 2 frequency bands. The probability of the clustering index at each frequency bin was calculated to decide robust frequency range (Fig. 1c). Since the probability of the intermediate frequency band is uncertain, we defined both end frequency bands as the final 2 frequency bands: LF1, 0.03~0.08 Hz and LF2, 0.009~0.012 Hz. The 101 connectivity matrices for each subject were averaged to the 2 connectivity matrices according to the 2 frequency bands. If the ICN efficiency was considered in an uncertain low frequency (ULF) between LF1 and LF2, there was an ICN with a statistically significant difference in ULF from LF1 or LF2, but the tendency of ICN efficiency to frequency was maintained (See Supplementary Fig. S4). Thus, we analyzed contribution of ICN to brain network integration only in LF1 and LF2.

Sparsity of the connectivity matrix. We constructed the connectivity matrices with 7 different sparsity levels (1%, 3%, 5%, 7%, 9%, 10% and 15%) because the sparsity level of connectivity matrix affects graph theoretic measures[54]. We decided upon a 5% sparsity level for further analysis because the sparsity levels surviving the minimum correlation value of 0.3 or greater were from 1% to 5% and the sparsity levels satisfying criteria for small-world properties [i.e. $k_{net} > \log(n)$[55]] were from 5% to 15% (See Supplementary Fig. S5).

ICN efficiency (E_{ICN}). We defined E_{ICN} to evaluate the contribution of ICN to brain network integration more directly. E_{ICN} was defined as

$$E_{ICN} = E_{Global} - E_{ICN^C} \tag{1}$$

$$E_{ICN^C} = \frac{1}{k_{ICN^C}} \sum_{i \in K_{ICN^C}} E_{i,\,ICN^C} = \frac{1}{k_{ICN^C}} \sum_{i \in K_{ICN^C}} \frac{\sum_{j \in K_{ICN^C}, j \neq i} d_{ij}^{-1}}{k_{ICN^C} - 1} \tag{2}$$

where, K_{ICN^C} is the set of all nodes in whole brain network except ICN, k_{ICN^C} is the number of K_{ICN^C}, and d_{ij} is the shortest path length between nodes i and j. E_{ICN} can detect the change of the shortest path length of the brain network when ICN was excluded and indicates the contribution of an individual ICN to brain network integration. Note that E_{ICN} cannot distinguish which region of the ICN affects the change of the contribution.

Betweeneess centrality (BC) hub. We investigated the number of BC hubs as the indicator of E_{ICN} together. The BC measurement of nodes is the rate at which each node passes through the shortest path between other nodes[56]. BC was defined as

$$BC(i) = \frac{1}{(k-1)(k-2)} \sum_{\substack{h,j \in K \\ h \neq j, h \neq i, j \neq i}} \frac{\rho_{hj}(i)}{\rho_{hj}} \tag{3}$$

where, K is the set of all nodes in the whole brain network, k is the number of K and ρ_{hj} is the number of the shortest paths between h and j, and $\rho_{hj}(i)$ is the number of the shortest paths between h and j that pass through i. BC can detect the extent to which particular regions of an ICN involve the shortest path lengths within a brain network. BC hub was determined as the node that was one standard deviation above the network average BC[12].

Efficiency between each ICN and the other ICNs ($E_{ICN-ICN}$). We computed the $E_{ICN-ICN}$ to investigate different integration with other ICNs of each sub-ICN along the frequency band. The $E_{ICN-ICN}$ is the shortest path length between ICN and other ICNs. $E_{ICN-ICN}$ was defined as

$$E_{ICN-ICN} = \frac{1}{k_{ICN_a} * k_{ICN_b}} \sum_{i \in K_{ICN_a}} \sum_{j \in K_{ICN_b}} d_{ij}^{-1} \tag{4}$$

where, K_{ICN} is the set of nodes of ICN, k_{ICN} is the number of K_{ICN} and d_{ij} is the shortest path length between nodes i in ICN_a and j in ICN_b. $E_{ICN-ICN}$ can detect how many shortest paths each ICN has with other ICNs.

Statistical evaluation. A paired sample t-test between the E_{ICN} of 2 frequency bands was performed to investigate whether the contributions of an ICN to brain network integration along the frequency bands were different from each other. The paired sample t-test of E_{ICN} was corrected by the significance level of p-value <0.005 with Bonferroni correction (Figs 2 and 5a). A paired sample t-test between the E_{ICN} of 2 frequency bands in sub-ICN was performed to investigate wheter the contributons of an ICN to brain network integration along the frequency bands were different from each other. The paired sample t-test of E_{ICN} in sub-ICN was corrected by the significance level of p-value <0.008 with Bonferroni correction (Figs 3 and 5b). Two sample t-test between the $E_{ICN-ICN}$ of sub-ICN pair was performed to investigate the different integration with other ICNs along the frequency bands. The two sample t-test of $E_{ICN-ICN}$ of sub-ICN was corrected by the significance level of p-value of 0.0025 with Bonferroni correction (Fig. 4).

References

1. Biswal, B., Zerrin Yetkin, F., Haughton, V. M. & Hyde, J. S. Functional connectivity in the motor cortex of resting human brain using echo-planar mri. *Magnetic resonance in medicine* **34**, 537–541 (1995).
2. Fox, M. D. & Raichle, M. E. Spontaneous fluctuations in brain activity observed with functional magnetic resonance imaging. *Nature Reviews Neuroscience* **8**, 700–711 (2007).
3. Beckmann, C. F., DeLuca, M., Devlin, J. T. & Smith, S. M. Investigations into resting-state connectivity using independent component analysis. *Philosophical Transactions of the Royal Society of London B: Biological Sciences* **360**, 1001–1013 (2005).
4. Damoiseaux, J. *et al.* Consistent resting-state networks across healthy subjects. *Proceedings of the national academy of sciences* **103**, 13848–13853 (2006).
5. Fox, M. D. *et al.* The human brain is intrinsically organized into dynamic, anticorrelated functional networks. *Proceedings of the National Academy of Sciences of the United States of America* **102**, 9673–9678 (2005).
6. Greicius, M. D., Krasnow, B., Reiss, A. L. & Menon, V. Functional connectivity in the resting brain: a network analysis of the default mode hypothesis. *Proceedings of the National Academy of Sciences* **100**, 253–258 (2003).
7. Hampson, M., Peterson, B. S., Skudlarski, P., Gatenby, J. C. & Gore, J. C. Detection of functional connectivity using temporal correlations in MR images. *Human brain mapping* **15**, 247–262 (2002).

8. Seeley, W. W. *et al*. Dissociable intrinsic connectivity networks for salience processing and executive control. *The Journal of neuroscience* **27**, 2349–2356 (2007).

9. Shirer, W., Ryali, S., Rykhlevskaia, E., Menon, V. & Greicius, M. Decoding subject-driven cognitive states with whole-brain connectivity patterns. *Cerebral cortex* **22**, 158–165 (2012).

10. Smith, S. M. *et al*. Correspondence of the brain's functional architecture during activation and rest. *Proceedings of the National Academy of Sciences* **106**, 13040–13045 (2009).

11. Chen, H. *et al*. Multivariate classification of autism spectrum disorder using frequency-specific resting-state functional connectivity—a multi-center study. *Progress in Neuro-Psychopharmacology and Biological Psychiatry* **64**, 1–9 (2016).

12. Sasai, S. *et al*. Frequency-specific network topologies in the resting human brain. *Frontiers in human neuroscience* **8** (2014).

13. Thompson, W. H. & Fransson, P. The frequency dimension of fMRI dynamic connectivity: Network connectivity, functional hubs and integration in the resting brain. *NeuroImage* **121**, 227–242 (2015).

14. Wu, C. W. *et al*. Frequency specificity of functional connectivity in brain networks. *Neuroimage* **42**, 1047–1055 (2008).

15. Mantini, D., Perrucci, M. G., Del Gratta, C., Romani, G. L. & Corbetta, M. Electrophysiological signatures of resting state networks in the human brain. *Proceedings of the National Academy of Sciences* **104**, 13170–13175 (2007).

16. Zuo, X.-N. *et al*. The oscillating brain: complex and reliable. *Neuroimage* **49**, 1432–1445 (2010).

17. Penttonen, M. & Buzsáki, G. Natural logarithmic relationship between brain oscillators. *Thalamus & Related Systems* **2**, 145–152 (2003).

18. van den Heuvel, M. P. & Pol, H. E. H. Exploring the brain network: A review on resting-state fMRI functional connectivity. *Eur Neuropsychopharm* **20**, 519–534, https://doi.org/10.1016/j.euroneuro.2010.03.008 (2010).

19. Latora, V. & Marchiori, M. Efficient behavior of small-world networks. *Physical review letters* **87**, 198701 (2001).

20. Latora, V. & Marchiori, M. Economic small-world behavior in weighted networks. *Eur Phys J B* **32**, 249–263, https://doi.org/10.1140/epjb/e2003-00095-5 (2003).

21. Rubinov, M. & Sporns, O. Complex network measures of brain connectivity: uses and interpretations. *Neuroimage* **52**, 1059–1069, https://doi.org/10.1016/j.neuroimage.2009.10.003 (2010).

22. Han, Y. *et al*. Frequency-dependent changes in the amplitude of low-frequency fluctuations in amnestic mild cognitive impairment: a resting-state fMRI study. *Neuroimage* **55**, 287–295 (2011).

23. Wang, Z. *et al*. Frequency-dependent amplitude alterations of resting-state spontaneous fluctuations in idiopathic generalized epilepsy. *Epilepsy research* **108**, 853–860 (2014).

24. Yu, R. *et al*. Frequency-specific alternations in the amplitude of low-frequency fluctuations in schizophrenia. *Human brain mapping* **35**, 627–637 (2014).

25. Postuma, R. B. & Dagher, A. Basal ganglia functional connectivity based on a meta-analysis of 126 positron emission tomography and functional magnetic resonance imaging publications. *Cerebral cortex* **16**, 1508–1521 (2006).

26. Vogt, B. A., Vogt, L. & Laureys, S. Cytology and functionally correlated circuits of human posterior cingulate areas. *Neuroimage* **29**, 452–466 (2006).

27. Leech, R., Braga, R. & Sharp, D. J. Echoes of the brain within the posterior cingulate cortex. *Journal of Neuroscience* **32**, 215–222 (2012).

28. Cha, J., Jo, H. J., Gibson, W. S. & Lee, J. M. Functional organization of the human posterior cingulate cortex, revealed by multiple connectivity-based parcellation methods. *Human Brain Mapping* **38**, 2808–2818 (2017).

29. Leech, R., Kamourieh, S., Beckmann, C. F. & Sharp, D. J. Fractionating the default mode network: distinct contributions of the ventral and dorsal posterior cingulate cortex to cognitive control. *The Journal of Neuroscience* **31**, 3217–3224 (2011).

30. Spielberg, J. M. *et al*. Trait approach and avoidance motivation: lateralized neural activity associated with executive function. *Neuroimage* **54**, 661–670 (2011).

31. Menon, V. & Uddin, L. Q. Saliency, switching, attention and control: a network model of insula function. *Brain Structure and Function* **214**, 655–667 (2010).

32. Taylor, K. S., Seminowicz, D. A. & Davis, K. D. Two systems of resting state connectivity between the insula and cingulate cortex. *Human brain mapping* **30**, 2731–2745 (2009).

33. Sridharan, D., Levitin, D. J. & Menon, V. A critical role for the right fronto-insular cortex in switching between central-executive and default-mode networks. *Proceedings of the National Academy of Sciences* **105**, 12569–12574 (2008).

34. Chang, C. & Glover, G. H. Time–frequency dynamics of resting-state brain connectivity measured with fMRI. *Neuroimage* **50**, 81–98 (2010).

35. Muller, K. *et al*. Investigating the wavelet coherence phase of the BOLD signal. *J Magn Reson Imaging* **20**, 145–152, https://doi.org/10.1002/jmri.20064 (2004).

36. Grinsted, A., Moore, J. C. & Jevrejeva, S. Application of the cross wavelet transform and wavelet coherence to geophysical time series. *Nonlinear Proc Geoph* **11**, 561–566, https://doi.org/10.5194/npg-11-561-2004 (2004).

37. Van Essen, D. C. *et al*. The Human Connectome Project: a data acquisition perspective. *Neuroimage* **62**, 2222–2231 (2012).

38. Glasser, M. F. *et al*. The minimal preprocessing pipelines for the Human Connectome Project. *Neuroimage* **80**, 105–124 (2013).

39. Smith, S. M. *et al*. Resting-state fMRI in the human connectome project. *Neuroimage* **80**, 144–168 (2013).

40. Salimi-Khorshidi, G. *et al*. Automatic denoising of functional MRI data: combining independent component analysis and hierarchical fusion of classifiers. *Neuroimage* **90**, 449–468, https://doi.org/10.1016/j.neuroimage.2013.11.046 (2014).

41. Power, J. D., Barnes, K. A., Snyder, A. Z., Schlaggar, B. L. & Petersen, S. E. Spurious but systematic correlations in functional connectivity MRI networks arise from subject motion. *Neuroimage* **59**, 2142–2154, https://doi.org/10.1016/j.neuroimage.2011.10.018 (2012).

42. Murphy, K., Birn, R. M., Handwerker, D. A., Jones, T. B. & Bandettini, P. A. The impact of global signal regression on resting state correlations: are anti-correlated networks introduced? *Neuroimage* **44**, 893–905, https://doi.org/10.1016/j.neuroimage.2008.09.036 (2009).

43. Biswal, B. B. *et al*. Toward discovery science of human brain function. *Proc Natl Acad Sci USA* **107**, 4734–4739, https://doi.org/10.1073/pnas.0911855107 (2010).

44. Chung, S. J. *et al*. Sleep Disturbance May Alter White Matter and Resting State Functional Connectivities in Parkinson's Disease. *Sleep* **40**, zsx009 (2017).

45. Park, H. *et al*. Agreement between functional connectivity and cortical thickness-driven correlation maps of the medial frontal cortex. *Plos One* **12**, https://doi.org/10.1371/journal.pone.0171803 (2017).

46. Lee, Y. *et al*. The cholinergic contribution to the resting-state functional network in non-demented Parkinson's disease. *Scientific Reports* **8**, https://doi.org/10.1038/s41598-018-26075-3 (2018).

47. Lee, Y. *et al*. Gender-specific effect of uric acid on resting-state functional networks in de novo Parkinson's disease. *Parkinsonism Relat Disord* **52**, 49–54, https://doi.org/10.1016/j.parkreldis.2018.03.023 (2018).

48. Kim, J. I. *et al*. Resting-state functional magnetic resonance imaging investigation of the neural correlates of cognitive-behavioral therapy for externalizing behavior problems in adolescent bullies. *Prog Neuro-Psychoph* **86**, 193–202, https://doi.org/10.1016/j.pnpbp.2018.05.024 (2018).

49. Jo, H. J., Saad, Z. S., Simmons, W. K., Milbury, L. A. & Cox, R. W. Mapping sources of correlation in resting state FMRI, with artifact detection and removal. *Neuroimage* **52**, 571–582 (2010).

50. Richiardi, J. *et al*. Correlated gene expression supports synchronous activity in brain networks. *Science* **348**, 1241–1244 (2015).

51. Torrence, C. & Compo, G. P. A practical guide to wavelet analysis. *Bulletin of the American Meteorological society* **79**, 61–78 (1998).
52. De Domenico, M., Nicosia, V., Arenas, A. & Latora, V. Structural reducibility of multilayer networks. *Nat Commun* **6**, https://doi.org/10.1038/ncomms7864 (2015).
53. De Domenico, M., Porter, M. A. & Arenas, A. MuxViz: a tool for multilayer analysis and visualization of networks. *Journal of Complex Networks* **3**, 159–176, https://doi.org/10.1093/comnet/cnu038 (2014).
54. Fornito, A., Zalesky, A. & Breakspear, M. Graph analysis of the human connectome: promise, progress, and pitfalls. *Neuroimage* **80**, 426–444 (2013).
55. Achard, S., Salvador, R., Whitcher, B., Suckling, J. & Bullmore, E. A resilient, low-frequency, small-world human brain functional network with highly connected association cortical hubs. *Journal of Neuroscience* **26**, 63–72 (2006).
56. Freeman, L. C. Centrality in Social Networks Conceptual Clarification. *Soc Networks* **1**, 215–239, https://doi.org/10.1016/0378-8733(78)90021-7 (1979).
57. Baria, A. T., Baliki, M. N., Parrish, T. & Apkarian, A. V. Anatomical and functional assemblies of brain BOLD oscillations. *The Journal of Neuroscience* **31**, 7910–7919 (2011).
58. Qian, L. *et al*. Frequency dependent topological patterns of resting-state brain networks. *PloS one* **10**, e0124681 (2015).

Acknowledgements

Author Contributions

Y.H.P. and J.M.L. designed the research. Y.H.P. performed data analysis. Y.H.P., J.C.,V.B. and J.M.L. wrote manuscript.

Additional Information

Supplementary information accompanies this paper at https://doi.org/10.1038/s41598-019-40699-z.

Competing Interests: The authors declare no competing interests.

Publisher's note: Springer Nature remains neutral with regard to jurisdictional claims in published maps and institutional affiliations.